A Novel IEPE AE-Vibration-Temperature-Combined Intelligent Sensor for Defect Detection of Power Equipment

A Novel IEPE AE-vibration-temperature Combined Intelligent Sensor for Defect Detection of Power Equipment

Zhaoyu Zhang, Haotian Wang, Huan Chen, Tianyi Shi, Yanfeng Song, Xutao Han, and Junhao Li, *Senior Member, IEEE*

***Abstract*—Insulation and mechanical defects are the main reasons of the power equipment fault, the former could generate partial discharge (PD) which can be detected by acoustic emission (AE) sensor, the other one can be evaluated by vibration and temperature variation. However, the two defects are detected and analyzed independently in traditional detection, the importance of multi-signal interaction and fusion analysis is ignored. To realize multi-signal synchronous detection and associated analysis, and improve the accuracy and efficiency of state evaluation of power equipment, a novel integrated electronics piezoelectric (IEPE) AE-vibration-temperature combined intelligent sensor is proposed and developed in this paper. Reasonable structure design and components customization enable the sensor to acquire signals simultaneously. Meanwhile, integrated transducer electronic data sheet (TEDS) and data processing circuit intelligentize the combined sensor. The primary detection parameters of the sensor are acquired in the calibration experiments. In PD, vibration and temperature joint experiment, it is verified that the combined sensor is more sensitive and multifunctional. Besides, a new fusion analysis diagram, vibration-phase resolved partial discharge (V-PRPD), is proposed to characterise the correlation between PD and vibration.**

***Index Terms*—power equipment, partial discharge, mechanical vibration, temperature, sensor.**

I. Introduction

LARGE power equipment, such as transformer, gas insulated substation (GIS), generator and motor, takes an important position in the development of society. Since the fault of the power equipment cost enormously, the operation condition evaluation is important and necessary. Power equipment is not only significant electrical equipment, but also complex mechanical equipment, which means its fault is primarily generated by typical insulation and mechanical defects, such as suspension and metal particle discharges, poor contact and winding deformation inside [1]–[6]. Actually, these two defects are correlative. Take GIS for example, under high electric field and constant mechanical vibration caused by electric force, loosened and poor contact could lead to suspension discharge, and metal particles produced by friction could lead to particle discharge and even creeping discharge [7], [8]. On the other hand, persistent PD around the contact could accelerate insulation deterioration and aging of contact segments, resulting in further thermal erosion and deformation [9]. Therefore, insulation and mechanical defects could exist simultaneously and influence each other, it is necessary to obtain effective information of the two defects to reasonably assess the power equipment operation condition.

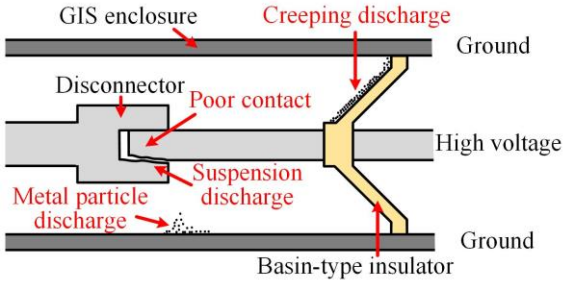

Fig. 1. Some correlative defects in GIS.

Ultrasound (frequency > 20 kHz) is one of the characteristic signals generated by PD, because it has high directionality and transmissibility, AE technology is widely used to locate PD and confirm the type in transformer, GIS as well as rotating electrical machines [10]. [11]–[13] illustrates the defect detection of GIS through investigation of theoretical and experimental basis, gathering field experiences and development of expert systems, and particle characterization in GIS. [14] proposes a particle-swarm-optimization route-searching (PSORS) algorithm for searching the position of the PD source in transformer. [15] classifies and analyzes the characteristics of different types of PD in insulation stator of the generator with AE sensor. Moreover, some papers focus on the intelligent statistical algorithms application in PD diagnosis, such as neural networks and acoustic amplitude flight time (AAFT) pattern [16], [17]. As for the mechanical defect, the equipment mechanical vibration is caused by current, while different equipment mechanical structure determines different vibration condition, when the structure changes due to mechanical defect, abnormal vibration occurs, so the vibration acceleration sensor (frequency < 4 kHz) is generally applied to detect mechanical defect in equipment [18]. [19] studies the vibration variation when GIS disconnector stays poor contact, declaring that high-frequency component of vibration signal on the enclosure increases significantly. Based on vibration signal, [20] applies operating deflection shapes (ODSs) to visualize the vibration patterns of power transformer windings mechanical condition. [21]

Manuscript received December 19, 2022; revised March 20, 2023; accepted April 6, 2023. This work was supported by 1.National Natural Science Foundation of China Joint Fund Key Project under Grant U22B20118, and 2.State Key Laboratory of Electrical Insulation and Power Equipment under Grant EIPE22128. *(Corresponding author: Junhao Li.)*

Zhaoyu Zhang, Haotian Wang, Huan Chen, Tianyi Shi, Yanfeng Song, Xutao Han, and Junhao Li are with the State Key Laboratory of Electrical Insulation and Power Equipment, Xi'an Jiaotong University, Xi'an 710049, China (e-mail: junhaoli@mail.xjtu.edu.cn)

proposes a Deep Belief Network (DBN)-based approach to extract features from vibration signals for evaluating induction motor working condition. In addition, mechanical defect and overload operation could lead to abnormal temperature rise, which can be also used to reflect the equipment operation condition [19]. Through enclosure and environmental temperature values, [22] inversely calculates 500 kV GIS contact temperature for reflecting contact thermal fault.

In previous studies, AE, vibration and temperature signals are usually detected and analyzed independently, the sensors are installed on the power equipment at different position, or at the same position alternatively, which is hard to ensure device uniformity and detection synchronization in space and time, and the correlation between signals cannot be studied easily [23]–[25]. On the other hand, it is accepted that the defect of equipment has different manifestation in different deterioration stage, multi-signal monitoring can help to observe the defect evolvement [26]. Therefore, the independent detection is not precise nor efficient for synchronous multi-signal fusion analysis to improve the accuracy of diagnosis, and the equipment operation condition cannot be evaluated comprehensively.

For defect detection of electrical equipment, the fushion signal detection and analysis is one of research focuses nowadays [27]–[30]. Specifically, AE and vibration signals could reflect insulation and mechanical states, and the temperature signal could be used to monitor the operation condition of some devices or compensate the temperature drift of sensor. Economically, combined sensor realizes multi-signal detection with few cost increasing, which is feasible for promotion; Conveniently, one kit detecting signals and saving data simultaneously can simplify the process and save time; Technically, synchronous multi-signal detection in time and space is the premise of fusion analysis which could evalute the equipment condition from aspects, improving the processability of data and detection efficiency.

In this paper, through proposing a new structure, fabricating mass-backing block and designing integrated signal conditioner, we develop a novel IEPE AE-vibration-temperature combined sensor which is able to acquire and preprocess the three signals synchronously. The output analog signal can be separated by filters to vibration acceleration signal (1 Hz ~ 4 kHz) and AE signal (above 20 kHz) for processing, and the digital signal is used to control the thermocouple and read TEDS of the sensor. The primary parameters of the combined sensor are given in calibration experiment, and the multi-signal joint detection experiment verifies the practicability of the combined sensor by comparing with the commercial sensors. It is declared that the combined sensor in this paper is made based on GIS defect detection, while it can be also applied on other equipment only if adjusting some detection parameters.

II. The IEPE Combined Intelligent Sensor

A. Structure and principle

AE sensor detection principle is based on acoustic matching principle and the piezoelectric effect resonant characteristic, while vibration acceleration sensor is based on the piezoelectric effect and Newton's second and third law of motion, and both of them could be realized through electromechanical conversion with piezoelectric material. Therefore, reasonable structure is the key of the combined sensor. As shown in Fig. 2 (a), the sensor proposed in this paper includes housing, PCB, mass backing, piezoelectric ceramic (PZT-5), thermocouple, acoustic matching layer and lead wire. The housing and matching layer are both grounded, which can shield the sensor from electromagnetic interference, and metal matching layer can better protect the piezoelectric ceramics.

PZT-5 is a kind of widely used piezoelectric ceramic with high piezoelectric coefficient and mechanical strength, superior and stable performance, well broadband electromechanical response, so the vibration and AE signals can be well detected. Basic parameters of the PZT-5 used in this paper are shown in table I.

TABLE I
BASIC PARAMETERS OF PZT-5

Name	Value	Name	Value
Diameter/mm	20	**Thickness/mm**	4
Resonant Frequency/kHz	500	**Young's Modulus/GPa**	51
Coupling Coefficient	k_{33}=0.59 k_{31}=0.55	**Relative Dielectric Constant**	1700
Mechanical Q	64	**Dielectric loss/%**	2~2.5
Piezoelectric Coefficients/pC/N	d_{33}=460 d_{31}=-190	**Curie Point/℃**	240

The frequency response of piezoelectric sensor is mainly determined by PZT-5 and the mass block. Taking GIS for example, since the characteristic bands of vibration and AE signals in GIS concentrate on 100 Hz ~ 4 kHz and 20 kHz ~ 100 kHz respectively [32], [33], and normally the working band of AE sensor is near the resonant frequency, while that of vibration sensor is less than one-fifth of the resonant frequency [34], [35]. Therefore, to meet the requirements of vibration and AE detection on GIS, the resonant frequency of the combined sensor should be theoretically around 60kHz. The resonant frequency f_n of the combined sensor can be calculated according to equation (1) [36]:

$$f_n = \frac{1}{2\pi} \times \sqrt{\frac{E_{33} \cdot \pi \cdot D_p^{\,2}}{4 \cdot n \cdot m_s \cdot t_p}} \tag{1}$$

Where, n, D_p, t_p, E_{33} and m_s represent the number (n=2), diameter, thickness, young's modulus of PZT-5 and mass of the mass backing. If m_s is designed as 14 g, the resonant frequency f_n of the combined sensor will be 60 kHz.

Since the gap of acoustic impedance between PZT-5 (generally 34 MRayl) and the object to be measured is inversely proportional to the ultrasonic transmission efficiency the matching layer is important for improving the efficiency of AE detection [37]. For example, the enclosure of GIS is aluminum alloy, which acoustic impedance is 14.7 MRayl, so the appropriate acoustic impedance should be about 22.35 MRayl according to equation (2):

$$Z_{\mathrm{m}} = \sqrt{Z_{\mathrm{p}} \times Z_{\mathrm{o}}} \tag{2}$$

where Z_{m}, Z_{p} and Z_{o} represent the acoustic impedances of the matching layer, PZT-5 and the object respectively. In this paper, the matching layer is made of titanium (22.7 MRayl),

its good mechanical strength is also good for vibration transmission.

The mass backing is the key component of the combined sensor. As shown in Fig 2 (b), its housing is made of high density steel (brass) with good conductivity, which makes the mass backing performs as the mass block when detecting the vibration [38]. On the other hand, the tungsten and epoxy mixture is inlaid in the conical mass backing interior by casting method, so it contacts PZT-5 directly and absorbs the penetrated ultrasound, reducing the echo interference significantly [39].

The signal transmission flow which includes combined sensor, preprocessor and tablet PC is described in Fig. 2 (c), in which there are two signal lines and a ground line. As for the blue line, AE and vibration signals transmit from PZT-5 to PCB 1 which preprocesses the analog signals. And the preprocessor provides a 4 mA constant current (CC) for PCB 1, it also realizes A/D conversion and delivers the signals to tablet PC. As for the red line, the hot-junction of T-thermocouple is embedded in the matching layer around the PZT-5 to detect the temperature which can be also used to compensate the temperature drift of the PZT-5. The cold-junction of T-thermocouple is connected to PCB 2 where there are two 1-wire chips: thermocouple-to-digital converter (TDC) and TEDS which is a kind of EEPROM. Both the two chips are controlled by MCU in preprocessor and tablet PC. Besides, only the housing of the combined sensor is grounded, this single ground can avoid the possible influence of induced voltage on the detection object.

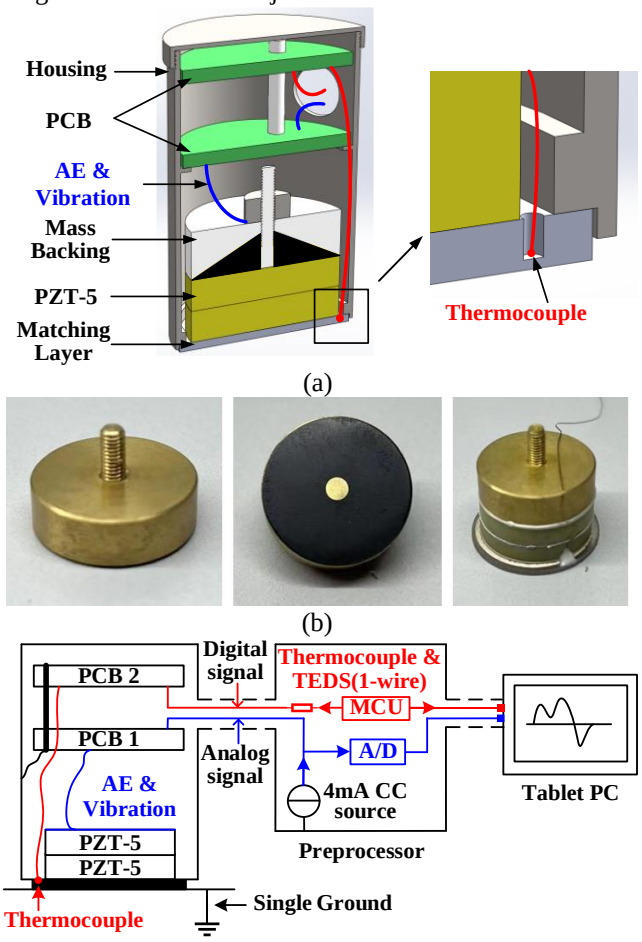

(c)

Fig. 2. The design of the combined sensor. (a) The structure. (b) The mass backing. (c) The signal transmission flow.

B. Integrated conditioning circuit

The integrated conditioning circuit consists of PCB 1 and PCB 2, they are connected by ground rod.

(1) PCB 1

The output voltage of PZT-5 should be preprocessed to acquire better transmission efficiency. The output impedance of PZT-5 is high (MΩ level), which makes the voltage hard to be collected [40], and the high frequency electromagnetic noise would interfere the signal of combined sensor. Therefore, the PCB 1 not only needs to convert the high output impedance to low, but also realizes amplification and wave filtering of the signal, improving the sensitivity and reducing the noise.

The designed schematic and practical sample of PCB 1 are shown in Fig. 3 (a) and (b). The JFET is used to convert the impedance of PZT-5 to low because of its fantastic impedance conversion characteristic, and the BJT is used to amplify the signal from JFET. Both JFET (common S) and BJT (common C) circuits have a reverse phase voltage output, so the phases of output and input of PCB 1 are consistent. Besides, C1 and C2 are used to remove low and high frequency noise respectively. Constant current source supplies 4 mA for PCB 1 which has a small output impedance, so the output actually consists of preprocessed signal and a DC bias voltage (generally 9 ~ 11 V). Therefore, the power and output share one line, simplifying the circuit to a great extent. In addition, the output signal would be then filtered by low pass and high pass filters (Cut off frequencies: 5 kHz & 18 kHz) in tablet PC to separate the vibration and AE signals for further analysis.

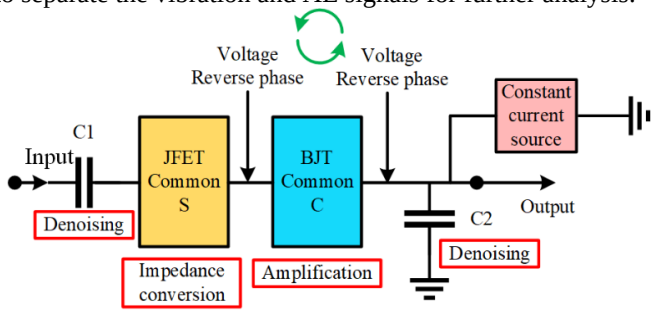

(a)

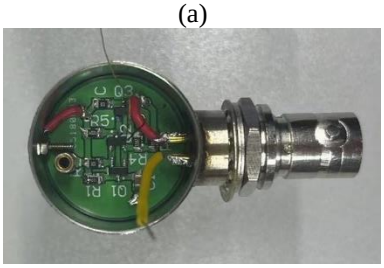

(b)

Fig. 3. The integrated conditioning circuit PCB 1. (a) The circuit topology. (b) The practical sample.

The simulation and experiment results of the PCB 1 are shown in Fig. 4. The magnifications of simulation and

experiment are around 17.2 and 18.3, and the cut-off frequencies are 133 kHz and 142 kHz respectively, the difference exists because the circuit parameters are slightly different, and the practical circuit environment is not ideal.

Above all, the PCB 1 designed for the combined sensor has 4 features:

(1) The input impedance is 1 GΩ for better receiving the signal from PZT-5, and output impedance changes in 20 Ω ~ 1000 Ω as input signal, the impedance of PZT-5 is converted to a low value.

(2) The circuit has a small number of components, which means good stability and minimal noise.

(3) The magnification (under 100kHz) could be adjusted by changing the resistances of BJT (common C) circuit according to application requirement.

(4) The cut-off frequency of filters can be adjusted as application requirement.

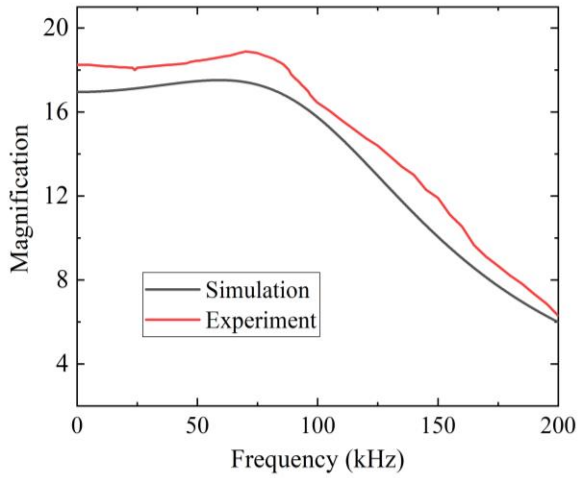

Fig. 4. The frequency response of the PCB 1.

(2) PCB 2

The PCB 2 is designed to control the thermocouple and store TEDS of the sensor for user to check before detection. To realize the two functions and minimize the number of signal line, 1-wire chip which works based on parasite power is used. On the one hand, TDC digitalizes the signal of thermocouple so that the temperature of the matching layer can be read. On the other hand, TEDS stores some primary parameters of the sensor, including the information of PCB, AE, vibration and temperature detection parameters. The circuit of PCB 2 is shown in Fig. 5.

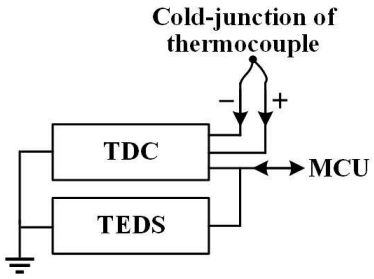

(a)

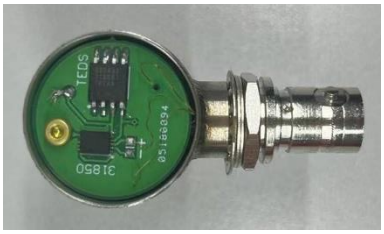

(b)

Fig. 5. The integrated conditioning circuit PCB 2. (a) The circuit topology. (b) The practical sample.

C. Assembly and detection device

The practical detection device and the combined sensor are shown in Fig. 6. The combined sensor is assembled by the components with conductive silver adhesive. And the detection software is developed on the tablet PC, so the AE, vibration acceleration, temperature signals and the information of the sensor can be read directly.

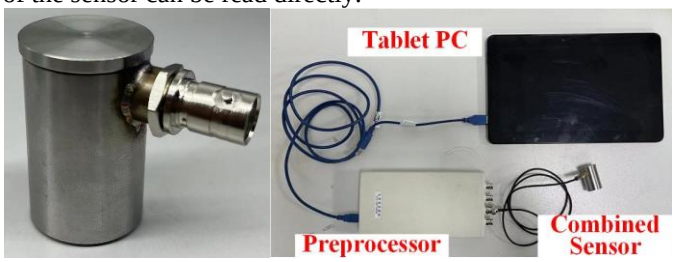

(a) (b)

Fig. 6. The combined sensor and detection system. (a) The combined sensor. (b) The detection device.

III. Calibration Experiment

It is important to confirm the working range of the combined sensor before calibration. The PD in GIS and the vibration on GIS generally distribute in 100 Hz ~ 4 kHz and 20 kHz ~ 100 kHz which are calibration bands in this paper [32], [33]. And the temperature calibration range is 25 ~ 80 ℃ which is enough for most experiment environment.

A. AE calibration

AE detection performance of the combined sensor is acquired according to ISO 12714:1999 [41]. The frequency response of the sensor under testing (SUT) can be calculated through a reference sensor (RS) determined by primary calibration. AE calibration experiment is shown in Fig 7. The diameter and height of the steel block are 42 cm and 21 cm respectively, the pencil-lead-break source producing the Rayleigh wave is mounted at the center of the block surface. While the SUT and RS are placed with ultrasonic coupling agent at equal distances (10 cm) from the source in opposite directions. Because of the symmetry of the sensor placement, the free surface displacement at the locations of the RS and SUT are equal. The signals of the two sensors are simultaneously recorded by oscilloscope and then processed by computer.

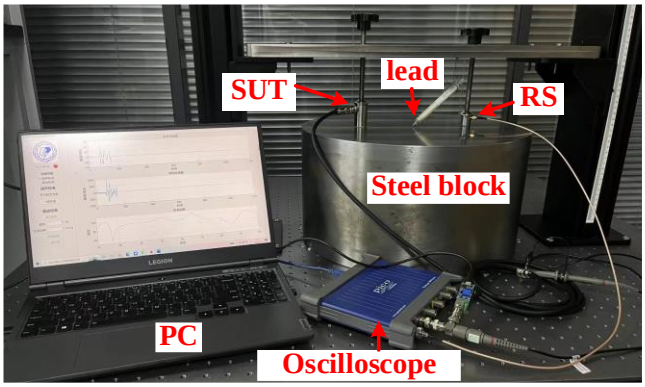

Fig. 7. AE calibration experiment.

The frequency response of SUT can be calculated by equation (3):

$$S_2(f) = 20 \times \log_{10} \frac{U_2(f)}{U_1(f)} + S_1(f) \tag{3}$$

where $S_1(f)$ and $S_2(f)$ represent the voltage sensitivity/dB (Ref 1V/(m/s)) of the RS and SUT respectively, and $U_1(f)$ and $U_2(f)$ are the output voltages in frequency domain of the two sensors. $S_1(f)$ is provided by the manufacturer of RS. The AE calibration result of combined sensor is shown in Fig. 8.

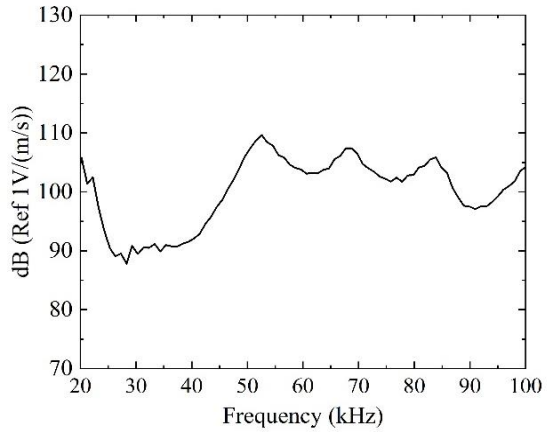

Fig. 8. The result of AE calibration.

The resonant frequency of the combined sensor is 54 kHz, the sensitivity reaches above 90 dB between 20 kHz ~ 100 kHz, and the average sensitivity is about 101 dB.

B. Vibration calibration

Vibration acceleration detection performance of the combined sensor is acquired according to ISO 16063-21:2003 [42]. The vibration calibration principle is similar as the AE calibration. Through exciting an adjustable vibration source to both the SUT and RS, the sensitivity of the SUT can be compared and calculated. The vibration calibration experiment is shown in Fig. 9.

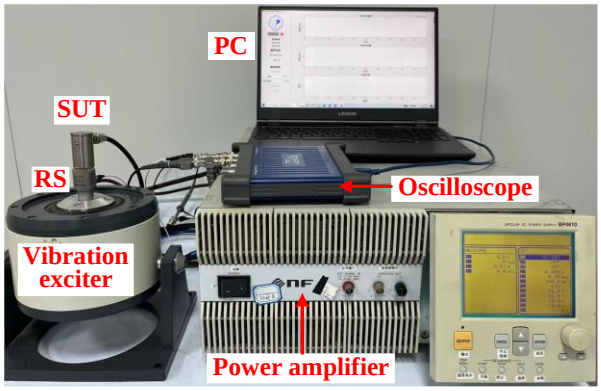

Fig. 9. Vibration calibration experiment.

The RS and SUT are fixed face-to-face on a standard vibration exciter to ensure that they receive the same vibration, and the vibration exciter is excited by sine wave power amplifier from 100 Hz to 4 kHz. The voltage sensitivity (mV/g) of the SUT can be calculated by the following equation (4), where $S_1(f)$ and $S_2(f)$ represent the voltage sensitivity of the RS and SUT respectively, and $U_1(f)$, $U_2(f)$ are output voltage amplitudes of the two sensors.

$$S_2(f) = \frac{U_2(f)}{U_1(f)} \times S_1(f) \tag{4}$$

The vibration calibration result of combined sensor is shown in Fig. 10, in which the vibration sensitivity is around 2000 mV/g in 100 Hz ~ 4 kHz band.

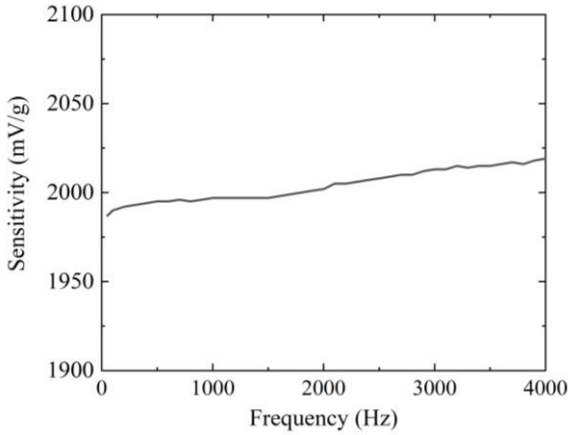

Fig. 10. The result of vibration calibration.(g ≈ 9.8m/s^2)

C. Temperature calibration

The temperature calibration experiment is shown in Fig. 11 (a). The combined sensor and a standard thermocouple (measured by thermometer) are pasted together and put in a digital thermotank. Therefore, comparing the temperatures of the combined sensor and the thermometer, the temperature detection parameter of the sensor can be calibrated. In this experiment, the thermotank rises temperature from 25 ℃ to 80 ℃.

In Fig.11 (b), it is clear that the combined sensor has a good temperature measurement performance as well as the standard thermocouple. The temperature of the combined sensor is slightly less than that of the standard thermocouple by around

1.1 ℃, because standard thermocouple measures directly the matching layer surface, while the thermocouple in combined sensor measures the matching layer inside, the thermal conduction leads to the loss. therefore, it is necessary to compensate the combined sensor temperature measurement with 1.1 ℃.

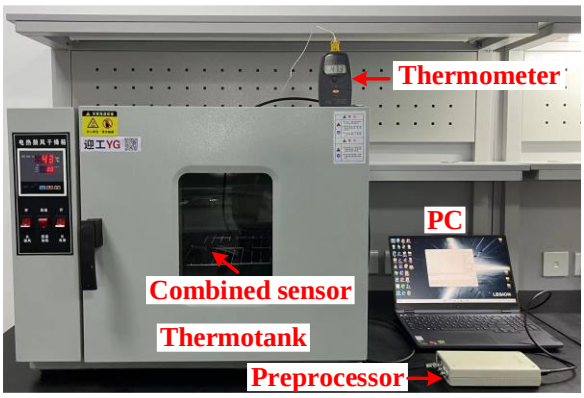

(a)

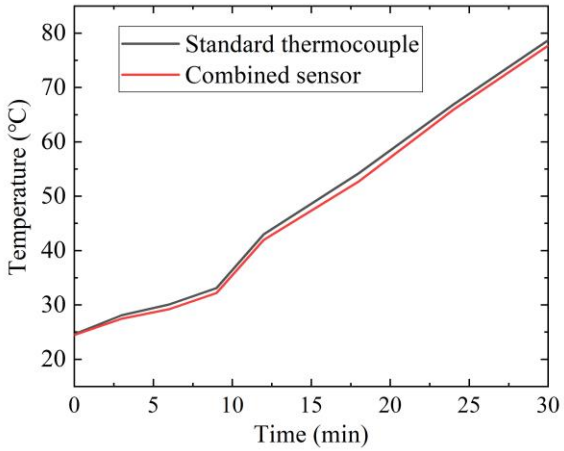

(b)

Fig. 11. Temperature calibration. (a) Temperature calibration experiment. (b)The result.

D. Other performances

To further verify reliability of the combined sensor, some important performances are also tested in laboratory and the result is shown in Table II.

TABLE II
SOME IMPORTANT PERFORMANCES OF THE COMBINED SENSOR

Name	Value (Vib)	Value (AE)	Value (Temp)
Hysteresis/%	0.06	0.07	0.5
Linearity/%	0.09	0.11	0.25
Repeatability/%	0.2	0.26	0.5
Precision/%	0.227	0.29	0.75
Resolution	0.025 m/s²	/	0.2℃
Uncertainty of calibration/%	0.68	0.74	0.58

IV. PD & VIBRATION & TEMPERATURE JOINT DETECTION EXPERIMENT

A. Experiment platform

In most abnormal condition, there could be both mechanical and insulation defects in power equipment. To verify the combined sensor performance for detecting AE, vibration and temperature signals synchronously, the multisource experiment platform is constructed with PD, vibration and heat sources.

As shown in Fig. 12, a typical PD defect (metal particle discharge) is installed in a pot sealed with 0.4 MPa SF_6 for insulation, which has a high voltage ball electrode at the top and a ground electrode at the bottom. The PD pot is fixed on the vibration exciter controlled by power amplifier. On one hand, high voltage is applied on the high voltage electrode to attract the particle to jump, when the particle falls back to the ground, the discharge happens to generate AE signal. On the other hand, the sealed pot vibrates as the vibration exciter. As for the temperature, a digital heater pad is pasted around the combined sensor to rise temperature. Besides, the combined sensor, commercial vibration sensor (CVS) and commercial AE sensor (CAS) are fixed on the bottom of the PD pot to detect the signals. The parameters of the three sensors are shown in TABLE III.

TABLE III
THE BASIC PARAMETERS OF THE SENSORS IN EXPERIMENT

Basic parameters		Combined Sensor	CVS	CAS
Band/Hz		50 ~ 4 k & 20 k ~ 100 k	1 ~ 5 k	25 k ~ 70 k
Sensitivity	Vib	2000 mV/g	103 mV/g	/
	AE	110 dB (peak)	/	80 dB (peak)
Resonant Frequency/Hz		54 k	>40 k	29 k
Temperature measurement/℃		25 ~ 80	/	/

To acquire clear result, there is only one metal particle in PD pot. The AE signal can be detected only when the experiment voltage is high enough to enable the metal particle to jump, and the start-jump voltage is 11 kV AC. The vibration exciter outputs 100 Hz sinusoidal vibration with 0.13 g, which is generally the major vibration on practical GIS enclosure [4]. Moreover, the digital heater pad is set to rise from 25 ℃ to 80 ℃ .

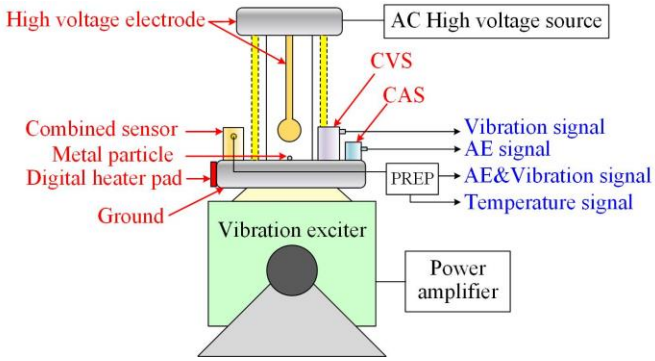

Fig. 12. The multi-source experiment platform.

B. Result and Analysis

The AE and vibration signals in time domain of the three sensors are shown in Fig. 13. It is observed that the combined sensor detects 100 Hz vibration and PD (impulses) signals, while the CVS and CAS only acquires 100 Hz vibration and PD signal respectively. To be specifically, The output voltage of combined sensor and CVS are around 260 mV and 13 mV which means the vibration is 0.13 g. On the other hand, the output of the combined sensor is 6 times than that of CAS.

The combined sensor is more sensitive than the two commercial sensors.

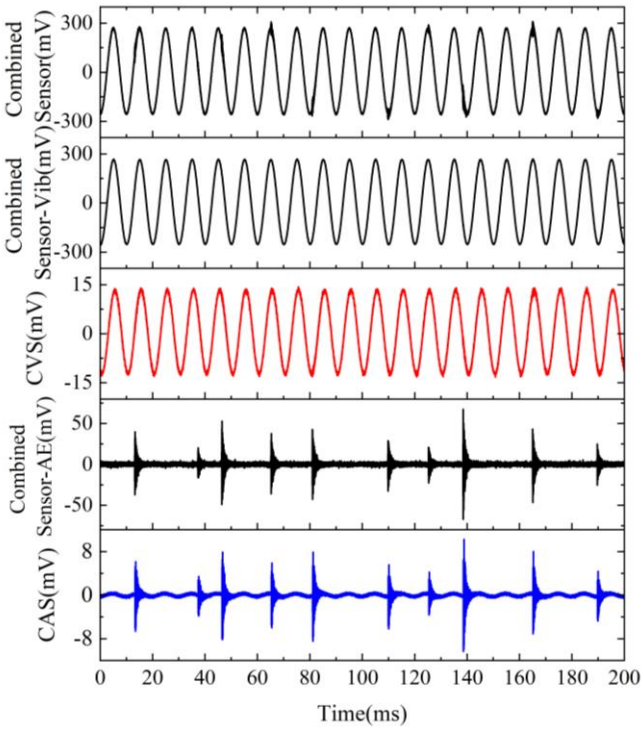

Fig. 13. The signals in time domain of the three sensors.

The frequency domain spectrum (FDS) of the three sensors is displayed in Fig. 14. For low band, it can be found that the combined sensor and CVS have the same low frequency features (100 Hz and 0.13 g), which is not clear for CAS.

As for the high frequency band, the combined sensor and CAS share similar distribution characteristic that the peak maximum appears at around 23 kHz, while they are different in rest of the band because the AE signals they detect are not totally duplicate and they have different frequency response shape in 20 kHz~100 kHz band. However, the CVS cannot acquire any effective information.

The above has verified that the combined sensor is able to detect vibration and AE signals better than commercial sensors, the synchronous detection is fundamental for fusion analysis. For example, the mechanical defect is one of the reasons for insulation defect in high voltage equipment. However, it is hard to determine how much the relationship is between the mechanical and insulation defects through single signal. Because the mechanical and insulation states can be reflected by vibration and AE signals respectively, the fusion analysis based on these two synchronous signals is supposed to solve this problem.

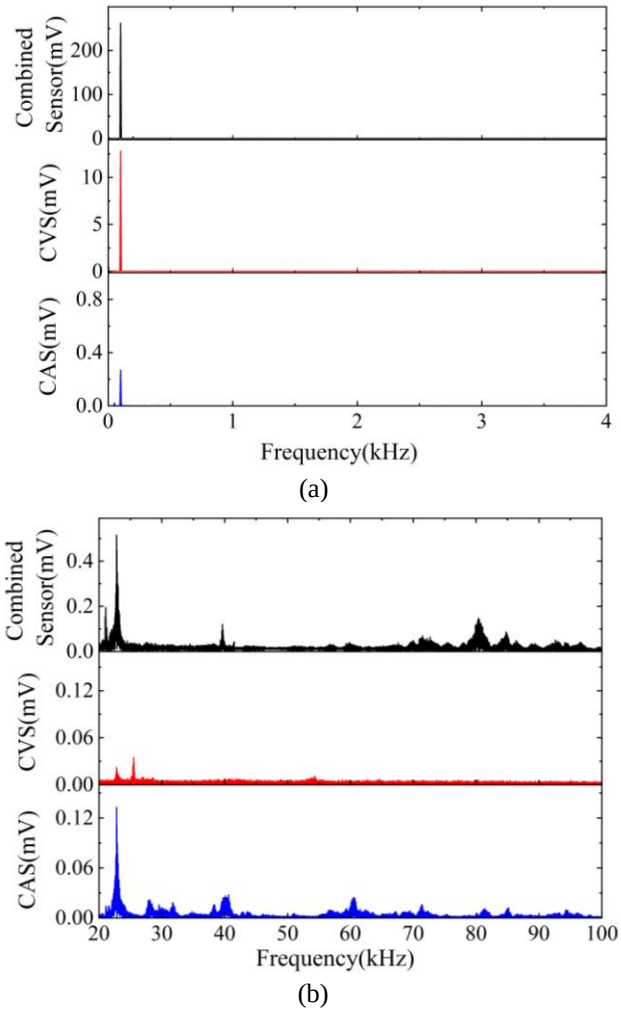

Fig. 14. The signals in frequency domain of the three sensors.

PRPD (Phase Resolved Partial Discharge), a PD statistic diagram based on 50 Hz AC voltage phase, is usually used to estimate PD type [43]. Similarly, based on the phase of 100 Hz vibration on equipment, we propose V-PRPD (Vibration-Phase Resolved Partial Discharge) to analyze if PD is affected by vibration. To get the V-PRPD, the combined signal is filtered firstly to vibration and AE signals (like combined sensor-vib and combined sensor-AE in Fig. 13). Comparing the two signals, the amplitude of every PD and corresponding vibration phase can be recorded, and the data volume in 1 s is enough for plotting V-PRPD. In this case, AC voltage is still 11 kV, and the vibration is set to 0.26 g, with the same data, PRPD and V-PRPD are displayed in Fig. 15.

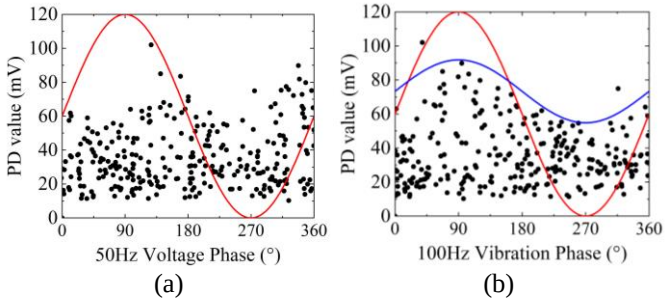

Fig. 15. PRPD and V-PRPD.

In Fig. 15 (a), the red line indicates one cycle of 50 Hz AC high voltage, while in Fig. 15 (b), the red line indicates one cycle of 100 Hz vibration generated from vibration exciter, both the red lines are used for phase reference. Besides, the black dot represents max value of every PD impulse, and the blue line is used to describe the envelope of black dots. In PRPD, PD peaks concentrate at 170° and 340° with a value of around 90 mV, showing two peaks distribution characteristic. Yet in V-PRPD, PD envelope (blue line) is clearly similar as the 100Hz vibration (red line) in phase which means the metal particle discharge is primarily dominated by the vibration. Specifically, the PD peak amplitude increases to around 90 mV when the PD pot vibrates up to the peak, and drops to 55 mV when the PD pot vibrates down to the peak. Therefore, V-PRPD, a new fusion analysis diagram plotted by 100 Hz vibration and AE impluses signal (PD), can be used to reflect the correlation between vibration and PD.

The temperature measurement result is shown in Fig.16, in which the temperatures of digital heater pad and the combined sensor rise from 25 ℃ to 80 ℃ in 35 minutes and then remain. The two lines are in good agreement, and the maximum relative error is 0.7 %, indicating that the combined sensor performs well on surface temperature measurement.

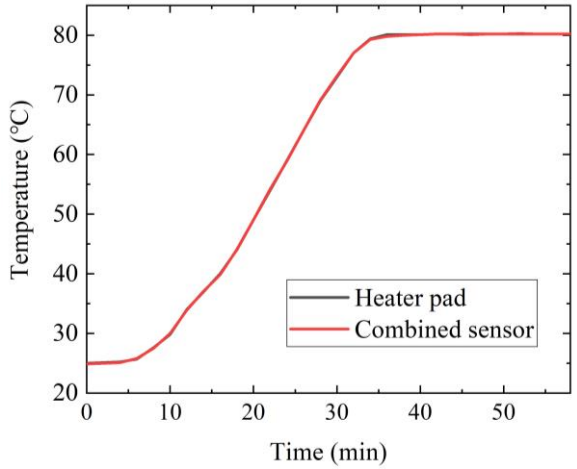

Fig. 16. Temperature measurement result.

V. Conclusion

In this paper, a novel IEPE AE-vibration-temperature combined sensor is proposed and developed to synchronously detect the PD and mechanical defect of power equipment. The designed structure and components realize the conversion from vibration and AE signals to voltage, and the integrated conditioning circuit helps to preprocess vibration and AE signals, digitize temperature and store TEDS. Through calibration experiments, the primary parameters of the combined sensor are 2 V/g for vibration, 110 dB (peak) for AE and 1.1 ℃ minus-deviation for temperature. On the other hand, the multisource experiment verifies the combined sensor is able to accurately acquire the simultaneous vibration, AE and temperature signals as good as commercial sensors, which is of practical significance for condition monitoring of power equipment. Besides, a new fusion analysis diagram (V-PRPD) is proposed, it could be used to assess the correlation between PD and vibration defect for PD reason.

In the future, aiming for the real defect detection in practical power equipment with the combined sensor, we decide to research for multi-signal feature extraction, fusion analysis and defect diagnosis from time domain, frequency domain and time-frequency domain. Statistic algorithms and sensor optimization will be the key of next research.

References

[1] C. -J. Chou and C. -H. Chen, "Measurement and analysis of partial discharge of high and medium voltage power equipment," *2018 7th International Symposium on Next Generation Electronics (ISNE)*, 2018, pp. 1-4.

[2] L. J. Wang *et al*., "Experimental investigation of typical partial discharge signals in medium-voltage switchgear," *2014 International Symposium on Discharges and Electrical Insulation in Vacuum (ISDEIV)*, 2014, pp. 393-396.

[3] M. Ren, C. Zhang, M. Dong, Z. Xiao and A. Qiu, "Partial discharges triggered by metal-particle on insulator surface under standard oscillating impulses in SF6 gas," in *IEEE Transactions on Dielectrics and Electrical Insulation*, vol. 22, no. 5, pp. 3007-3018, October 2015.

[4] J. Hao, Y. Ding, Y. Li, X. Li, X. Jiang and H. Peng, "Comparative Analysis of Partial Discharge and Mechanical Vibration Characteristics under Loose Bus Base with Foreign Body Defect of GIS," *2022 IEEE International Conference on High Voltage Engineering and Applications (ICHVE)*, 2022, pp. 1-4.

[5] Y. Zhong, J. Hao, X. Wang, R. Liao, R. Gong and Y. Ding, "Novel classification method of mechanical defects for GIS equipment based on mode function analysis and improved relevance vector machine," in *CSEE Journal of Power and Energy Systems*, early access, doi: 10.17775/CSEEJPES.2021.03580.

[6] S. Bagheri, Z. Moravej and G. B. Gharehpetian, "Classification and Discrimination Among Winding Mechanical Defects, Internal and External Electrical Faults, and Inrush Current of Transformer," in *IEEE Transactions on Industrial Informatics*, vol. 14, no. 2, pp. 484-493, Feb. 2018.

[7] Kai Wu *et al*., "Effect of mechanical vibration on the behavior of partial discharges in generator windings," in *IEEE Transactions on Dielectrics and Electrical Insulation*, vol. 13, no. 2, pp. 345-352, April 2006.

[8] L. Ma *et al*., "Study on the PD Creeping Discharge Development Process Induced by Metallic Particles in GIS," *2020 IEEE International Conference on High Voltage Engineering and Application (ICHVE)*, 2020, pp. 1-4.

[9] W. G. Moore and A. Khazanov, "Insulation degradation in generator stator bars due to spark erosion and partial discharge damage," *2010 IEEE International Symposium on Electrical Insulation*, 2010, pp. 1-5.

[10] H. D. Ilkhechi and M. H. Samimi, "Applications of the Acoustic Method in Partial Discharge Measurement: A Review," in *IEEE Transactions on Dielectrics and Electrical Insulation*, vol. 28, no. 1, pp. 42-51, February 2021.

[11] L. E. Lundgaard, M. Runde and B. Skyberg, "Acoustic diagnosis of gas insulated substations: a theoretical and experimental basis," in *IEEE Transactions on Power Delivery*, vol. 5, no. 4, pp. 1751-1759, Oct. 1990.

[12] L. E. Lundgaard, G. Tangen, B. Skyberg and K. Faugstad, "Acoustic diagnoses of GIS; field experience and development of expert system," in *IEEE Transactions on Power Delivery*, vol. 7, no. 1, pp. 287-294, Jan. 1992

[13] L. E. Lundgaard, "Particles in GIS characterization from acoustic signatures," in *IEEE Transactions on Dielectrics and Electrical Insulation*, vol. 8, no. 6, pp. 1064-1074, Dec. 2001.

[14] Y. -B. Wang *et al*., "Acoustic localization of partial discharge sources in power transformers using a particle-swarm-optimization-route-searching algorithm," in *IEEE Transactions on Dielectrics and Electrical Insulation*, vol. 24, no. 6, pp. 3647-3656, Dec. 2017.

[15] Y.-M. Yang and X.-J. Chen, "Partial Discharge Ultrasonic Analysis for Generator Stator Windings," *Journal of Electrical Engineering and Technology*, vol. 9, no. 2, pp. 670–676, Mar. 2014.

[16] Z. Wu, Q. Zhang, J. Song and X. Li, "Improved Method for Acoustic Identification of Free Conductive Particle Defects in GIL," in *IEEE Transactions on Power Delivery*, vol. 34, no. 4, pp. 1317-1323, Aug. 2019.

[17] Y. Tian, P. L. Lewin, A. E. Davies, S. J. Sutton and S. G. Swingler, "Application of acoustic emission techniques and artificial neural networks to partial discharge classification," *Conference Record of the*

the 2002 IEEE International Symposium on Electrical Insulation (Cat. No.02CH37316), 2002, pp. 119-123.
[18] M. Iorgulescu, R. Beloiu and M. O. Popescu, "Vibration monitoring for diagnosis of electrical equipment's faults," *2010 12th International Conference on Optimization of Electrical and Electronic Equipment*, 2010, pp. 493-499.
[19] M. Li, J. Bai, H. Xia, L. Xu, D. Ding and C. Ren, "Test Research on Poor Contact Defect Detection of GIS Based on Temperature and Vibration," *2020 IEEE 1st China International Youth Conference on Electrical Engineering (CIYCEE)*, 2020, pp. 1-5.
[20] Y. Shi, S. Ji, F. Zhang, Y. Dang and L. Zhu, "Application of Operating Deflection Shapes to the Vibration-Based Mechanical Condition Monitoring of Power Transformer Windings," in *IEEE Transactions on Power Delivery*, vol. 36, no. 4, pp. 2164-2173, Aug. 2021.
[21] S. Shao, W. Sun, P. Wang, R. X. Gao and R. Yan, "Learning features from vibration signals for induction motor fault diagnosis," *2016 International Symposium on Flexible Automation (ISFA)*, 2016, pp. 71-76.
[22] M. Yu-long, L. Chen, Y. Qiang, T. Ju and Z. Fu-ping, "Contact Temperature Monitoring and Layout Optimization of Shell Temperature Sensor of 500kV GIS," *2020 IEEE International Conference on High Voltage Engineering and Application (ICHVE)*, 2020, pp. 1-4.
[23] B. Liu, H. Ma and P. Ju, "Partial discharge diagnosis by simultaneous observation of discharge pulses and vibration signal," in *IEEE Transactions on Dielectrics and Electrical Insulation*, vol. 24, no. 1, pp. 288-295, Feb. 2017.
[24] I. K. Solin, O. Yolanda and R. Siregar, "Partial discharge measurement and vibration monitoring on power transformer case study on power transformer with high level noise (75.22 dB)," *2009 IEEE 9th International Conference on the Properties and Applications of Dielectric Materials*, 2009, pp. 521-524.
[25] Y. P. Aksenov, I. V. Yaroshenko, A. V. Andreev and G. Noé, "On-line transformer diagnostic methods synergy based on discharge and vibration events measurements and location," *8th IEEE Symposium on Diagnostics for Electrical Machines, Power Electronics & Drives*, 2011, pp. 437-443.
[26] X. Han, J. Li, L. Zhang, P. Pang and S. Shen, "A Novel PD Detection Technique for Use in GIS Based on a Combination of UHF and Optical Sensors," in *IEEE Transactions on Instrumentation and Measurement*, vol. 68, no. 8, pp. 2890-2897, Aug. 2019.
[27] H. Wang, X. Zhang, X. Han, Y. Sun, H. Chen and J. Li, "A Novel Composite Sensor for Overvoltage and UHF Partial Discharge Measurement in GIS," in *IEEE Transactions on Power Delivery*, vol. 37, no. 6, pp. 5476-5479, Dec. 2022.
[28] Fang H R, Deng J, Chen D S, et al. "You can get smaller: A lightweight self-activation convolution unit modified by transformer for fault diagnosis," *Advanced Engineering Informatics*, vol. 55, no. 101890, Jan. 2023.
[29] Jangjoo M A, Allahbakhshi M, Mirzaei H R. "UHF sensors positioning on the power transformer tank to enhance the partial discharge localization accuracy," *Electric Power Systems Research*, vol. 218, no. 109174, May. 2023.
[30] Demirci M, Gözde H, Taplamacioglu M C. "Improvement of power transformer fault diagnosis by using sequential Kalman filter sensor fusion," *International Journal of Electrical Power & Energy Systems*, vol. 149, no. 109038, July. 2023.
[31] X. Han *et al*., "Partial Discharge Detection in Gas-Insulated Switchgears Using Sensors Integrated With UHF and Optical Sensing Methods," *IEEE Transactions on Dielectrics and Electrical Insulation*, vol. 29, no. 5, pp. 2026-2033, Oct. 2022.
[32] Y. Liu, Y. -y. Jia, J. -g. Yang, S. -q. Song, B. Wu and J. Li, "Research of mechanical state diagnosis techniques in GIS bus connector based on mechanical vibration," *2018 12th International Conference on the Properties and Applications of Dielectric Materials (ICPADM)*, 2018, pp. 682-685.
[33] Chien-Yi Chen, Cheng-Chi Tai, Ching-Chau Su, Ju-Chu Hsieh and Jiann-Fuh Chen, "GIS partial discharge examination and classification from the on-line measurements," *2008 International Conference on Condition Monitoring and Diagnosis*, 2008, pp. 412-415.
[34] M. Iorgulescu, R. Beloiu and M. O. Popescu, "Vibration monitoring for diagnosis of electrical equipment's faults," in *2010 12th International Conference on Optimization of Electrical and Electronic Equipment*, Brasov, Romania, 2010, pp. 493-499.
[35] Bohse J, Brunner A J. *Acoustic emission in delamination investigation*. Sawston, Cambridge, UK. Woodhead Publishing, 2008,pp. 217-277.
[36] M.-K. Lee *et al.*, "Design Optimization of Bulk Piezoelectric Acceleration Sensor for Enhanced Performance," *Sensors*, vol. 19, no. 15, p. 3360, Jul. 2019.
[37] V. T. Rathod, "A Review of Acoustic Impedance Matching Techniques for Piezoelectric Sensors and Transducers," *Sensors*, vol. 20, no. 14, p. 4051, Jul. 2020.
[38] S. K. Regueig, Z. Ghemari and T. Benslimane, "Extraction of the relative sensitivity model and improvement of the piezoelectric accelerometer performances," *2018 International Conference on Signal, Image, Vision and their Applications (SIVA)*, 2018, pp. 1-5.
[39] Zhang W, Jia H, Gao G, et al. "Backing layers on electroacoustic properties of the acoustic emission sensors," in *Applied Acoustics*, vol. 156, pp. 387-393, Dec 2019.
[40] Karbari S R, Mohanram S, Sriniketh S S, et al. "Signal conditioning circuits for low vibration signals using an array of piezoelectric sensors," in *Materials Today*: *Proceedings*, vol. 46, no. 6, pp. 2212-2220, Mar. 2021.
[41] Non-destructive testing-Acoustic emission inspection-Secondary calibration of acoustic emission sensors, ISO 12714:1999.
[42] Methods for the calibration of vibration and shock transducers - Part 21: Vibration calibration by comparison to a reference transducer, ISO 16063-21:2003.
[43] K. Firuzi, M. Vakilian, B. T. Phung and T. R. Blackburn, "Partial Discharges Pattern Recognition of Transformer Defect Model by LBP & HOG Features," in *IEEE Transactions on Power Delivery*, vol. 34, no. 2, pp. 542-550, April 2019.

Zhaoyu Zhang, was born in Yuncheng, Shanxi, China, in 1995. He received the M.S. degree in electrical engineering from Xi'an Jiaotong University, Xi'an, in 2020, where he is currently pursuing the Ph.D. degree with a focus on the intelligent sensing technology, fault detection and state evaluation for power equipment.

Haotian Wang was born in Xi'an, Shaanxi, China, in 1999. He received the B.Sc. degree in electrical engineering from Xi'an Jiaotong University, Xi'an in 2020, where he is currently pursuing the Ph.D. degree with a focus on the fault detection and state evaluation for gas-insulated switchgear equipment.

Huan Chen was born in Nanyang, Henan, China, in 1999. He received the B.Sc. degree in electrical engineering from China University of Petroleum (East China), Qingdao, in 2021, where he is currently pursuing the M.Sc. degree with a focus on fault detection and state evaluation for gas-insulated switchgear equipment.

Tianyi Shi was born in 2000. He received the B.Sc. degree in electrical engineering from Xi'an Jiaotong University, Xi'an, in 2022, where he is currently pursuing the M.S. degree with a focus on the intelligent sensing technology, fault detection and state evaluation for power equipment.

Yanfeng Song was born in Yantai, shandong, China, in 1997. In 2020, He received the B.Sc. degree in electrical engineering from Chongqing University. At present, he is studying for the master's degree in Xi'an Jiaotong University, mainly focusing on the detection and diagnosis technology of gas insulated switchgear.

Xutao Han was born in Xi'an, Shaanxi, China, in 1991. He received the B.Sc. and Ph.D. degrees in electrical engineering from Xi'an Jiaotong University, Xi'an, in 2013 and 2019, where he is currently a Research Assistant with a focus on the detective and diagnostic techniques for gas-insulated switchgear equipment.

Junhao Li (Senior Member, IEEE) was born in Xuchang, Henan, China, in 1980. He received the Ph.D. degree in electrical engineering from Xi'an Jiaotong University, Xi'an, China, in 2010.

He is currently a Professor with Xi'an Jiaotong University, where he is involved in the detective and diagnostic techniques for electrical equipment and new types of the test method for electrical equipment, etc.